JOURNAL OF AIRCRAFT
Vol. 43, No. 1, January–February 2006

# Induced Drag Reduction Using Aeroelastic Tailoring with Adaptive Control Surfaces

Terrence A. Weisshaar*
*Purdue University, West Lafayette, Indiana 47907-1282*
and
David K. Duke†
*Lockheed-Martin Company, Fort Worth, Texas 76101*

**This paper describes the use of full-span deforming control surfaces (including controlled chordwise cambering of the wing) to provide effective subsonic induced drag control with precise control of the spanwise lift distribution. Examples of these proposed controllers are smart, adaptive actuators for advanced unmanned air vehicle concepts. Reshaping the wing spanwise lift distribution with aeroelastic tailoring concepts is shown to reduce induced drag at high airspeeds. Active controllers such as conventional ailerons or leading-edge devices also reduce induced drag if they have a tailored spanwise deflection pattern; the required deflections of these surfaces depend on wing deformation and can be so large that they are not practical. Combining wing aeroelastic stiffness tailoring with active control surface design to create a "control-friendly structure" reduces induced drag and requires only small controller inputs. An exact solution for the actuator deflections to generate an elliptical lift distribution for the aeroelastic wing, for minimum induced drag, is discussed. A formal optimization problem is posed for cases in which multiple surfaces are used to control drag. This controller optimization solution is complicated because aeroelastic phenomena, such as control reversal, limit the effectiveness of some actuators at high speed.**

## Nomenclature

$[A_{ij}]$ = aerodynamic influence coefficient matrix
$[B_{ij}]$ = $[(1/q)[A_{ij}] - [C_{ij}]]$
$[C_{ij}]$ = wing structural flexibility matrix
$EI$ = bending stiffness
$[E_{ij}]$ = matrix relating flexible change in wing angle of attack to control surface deflection
$GJ$ = torsional stiffness
$g$ = $K/GJ$
$K$ = bending-torsion coupling
$k$ = $K/EI$
$M$ = bending moment or flight Mach number
$q$ = flight dynamic pressure, psi
$T$ = torsional moment
$U_\infty$ = freestream airspeed
$W_i$ = span of actuator segment, nondimensionalized with respect to the wing semispan
$w$ = vertical displacement of wing section
$[Z_{ij}]$ = diagonal matrix relating sectional change in wing apparent angle of attack to control surface deflection ($Z_{ii} = \partial\alpha_i/\partial\beta_i$)
$\alpha_r$ = rigid wing angle of attack, radians
$\beta_i$ = control surface deflection at each wing section, radians
$\gamma$ = primary stiffness angle of single lamina with respect to spanwise reference axis (+ clockwise)
$\delta$ = induced drag parameter
$\varepsilon/c$ = vertical displacement of chordwise wing centroid in active parabolic wing cambering, nondimensionalized with respect to the local chord
$\theta$ = wing sectional twist
$\upsilon$ = weighted actuator effort parameter $\left(\sqrt{\sum_i W_i \beta_i^2}\right)$
$\psi^2$ = $K^2/(EI \cdot GJ)$
$\{1\}^T$ = row vector of ones

Presented as Paper 2000-1619 at the AIAA/ASME/ASCE/AHS/ASC 41st Structures, Structural Dynamics and Materials Conference, Atlanta, GA, 20–25 April 2000; received 29 July 2004; revision received 6 July 2004; accepted for publication 13 August 2004. 

*Professor, School of Aeronautics and Astronautics, 1282 Grissom Hall. Fellow AIAA.
†Senior Aeronautical Engineer.

## Introduction

IN addition to its importance for high-speed fighter maneuvers, small drag reductions provide worthwhile increases in airplane range or airplane loiter time. Our goal is to combine aeroelastic tailoring with active control surface deformation to create a "user-friendly structure" to host an active control system that reshapes the wing spanwise lift distribution to reduce induced drag.

Reference 1 explores how and under what circumstances combining aeroelastic tailoring with actively controlled deformation can reduce wing subsonic, induced drag. That study was followed by another described in Ref. 2. The types of active deformation control considered in Ref. 2 were ailerons, leading-edge devices, and active cambering. This paper summarizes trailing-edge device (aileron) induced drag reduction. Aeroelastic tailoring is a term broadly applied to the intentional use of directional structural stiffness features to improve measures of structural or aircraft performance (not necessarily least weight). Tailoring is automatically applied when aircraft multidisciplinary optimization includes advanced composite material design variables such as laminate thickness, number of plies, and laminate orientation. The measures of performance are broad also, but they certainly include increased flutter speed and lift effectiveness. Figure 1 summarizes multidisciplinary benefits of laminate tailoring or stiffness orientation.[3] The structural reference axis shown is the conventional wing structure elastic axis running outward along the swept wing itself. The term "primary stiffness" refers to the locus of points where the structure exhibits the most resistance to bending deformation. This location can be tailored by laying out stiffeners, ribs, or skin to rotate the principal stiffness axis fore or aft of the conventional elastic axis. Aeroelastic tailoring objectives in Fig. 1 conflict; a designer needs a formal optimization procedure to balance multidisciplinary conflicts or requirements for a specific design.

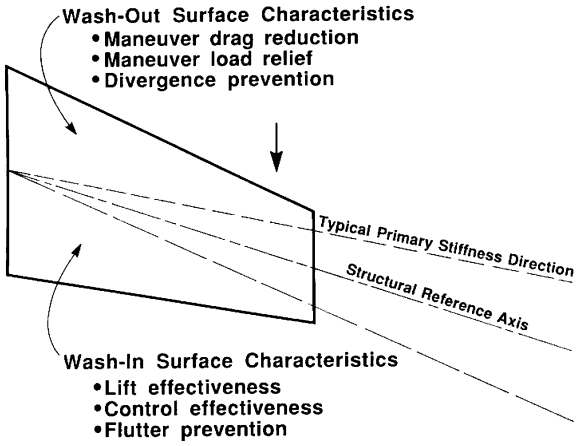


**Fig. 1 Laminate directional orientations to achieve selected aeroelastic performance.[1]**

Wash-out laminates are identified traditionally with drag reduction, although there is not an all-encompassing, published study of the effects of laminate orientation on wing-induced drag. The most comprehensive aeroelastic tailoring studies for fighter aircraft with performance constraints such as drag are from a group at General Dynamics, Ft. Worth (now Lockheed-Martin, Ft. Worth). Reference 4 is typical of their studies and their breadth of application.

The effects of aeroelastic distortion itself on induced drag have been known for at least 40 years,[5,6] and the effect of spanwise lift distribution itself has been recognized for 80 years. One of the oldest classical aerodynamic optimization problems is the spanwise distribution of lift required to produce minimum induced drag. This problem was addressed and solved by Munk in 1921; he showed that the wing planform shape with minimum drag was one that generated an elliptical lift distribution.[7] The elliptical lift distribution gives a constant downwash in the far-field wake. A succinct discussion of Munk's result is given by R. T. Jones.[8] He points out that the elliptical distribution solution is optimal only if the wing span is fixed.

Jones also discusses the optimization result that occurs when the wing structure has a structural strength constraint placed on it, but the wing span is allowed to increase or decrease. This problem, which Jones attributes to Prandtl, uses an averaged bending moment as a constraint. The result is that, with a limited bending moment, the downwash distribution in the far wake is parabolic, not uniform. These results show that induced drag can be reduced by extending the span and changing the chordwise geometry distribution (and presumably reducing the weight of the internal structure to support these loads). In all of our work to be discussed, the planform shape is fixed.

Designers routinely shape the wing lift distribution for minimum drag by tailoring the local "rigid" angles of attack along the wing to produce a low-drag lift distribution. This rigid twist distribution might not account for the aeroelastic effects of wing flexibility. Although the spanwise distribution of aerodynamic angle of attack (aerodynamic and geometric twist or "jig shape") determines the induced drag, a low-drag design is good only at a preselected design point. This design point is a combination of aircraft Mach number, altitude, and weight. Because aircraft weight, speed, and altitude change during flight operations, the wing design shape is optimal at only one mission design point. In addition, aeroelastic distortion will deoptimize the wing depending on the operational airspeed. Clearly, some active means is desirable to minimize drag throughout the operational flight envelope.

The idea of controlling aerodynamic performance by active, mechanically controlled distortion of wings is not new. For instance, in 1979, Elber[9] filed a patent entitled "Means for Controlling Aerodynamically Induced Twist." His controller was a long torque tube located inside the wing, extending from the actuator at the root to an attachment at the tip so that it could twist the wing tip and control swept-wing lift effectiveness. He did not claim to directly control drag.

At about the same time, programs like the Transonic Aircraft Technology Program[10–16] had performance optimization objectives involving limit load maneuvering; this required actively reshaping the spanwise lift distribution with an internal mechanism for chordwise wing bending to force variable camber shapes. Through camber control, drag polars were reshaped to reduce drag at operational airspeeds and to reduce critical wing bending moments.

Theoretically, the constant span drag-reduction objective translates into making the spanwise lift distribution as close to elliptical as possible, as long as strength requirements are not violated. This experiment was a great success, although the internal mechanisms required to for reshaping were heavy because they were designed to operate on an unmodified, stiff structure. Recently, a procedure to control drag by aileron/flap deflection on an L-1011 aircraft was tested by NASA Dryden Flight Research Center.[17] This procedure used real-time performance optimization and in-flight measurements to reduce drag on an L-1011 test aircraft. This scheme used a pair of symmetrical ailerons.

Two other innovative approaches to active/passive control of aerodynamic performance are worth mentioning. The first is the use of active materials and adaptive actuators for aeroelastically leveraged control. Advanced actuators, including piezoelectric devices with "smart" structures, have been proposed for small airplane control.[18] This control includes rolling and climbing, as well as control of transonic drag.[19] Second, there has been interest in improving lateral roll authority by intentionally reducing stiffness (the active flexible wing/active aeroelastic wing) and then controlling the aeroelastic response. This concept has been studied extensively for at least 15 years.[20–27] This aircraft control approach was also the subject of a patent filed by Tulinius in 1990 and granted in 1992 (Ref. 28). The intent of this effort is to provide a control system that is effective beyond the normal aileron reversal speed, not necessarily to focus on decreased drag itself.

Most formal multidisciplinary design-optimization efforts use aircraft component weight as an objective function and aircraft performance as a formal or implied constraint. Our study has three goals that make it different than previous studies. First of all, few studies have had as their objective the use of formal optimization methods to find structural planform configurations to reduce drag. We will demonstrate the effects of wing laminate design and its aeroelastic influence on induced drag. Finally, we will define a formal optimization problem to produce a wing/actuator design to reduce drag.

Our main findings are that, over a broad range of airspeeds, wing-induced drag can be reduced with either passive-wing aeroelastic tailoring, actively controlled actuators, or a combination. When used in combination, induced drag can be minimized with minimal actuator input if the structure is tailored properly. In addition, when a continuous full-span actuator is used, the required control deflections to reduce induced drag to a minimum can be determined from a closed-form problem solution, without formal optimization. Finally, we show that the formal optimization problem for drag reduction must have proper constraints to find the correct control deflections.

## Choice of Models

Wing structures are complex assemblages of interconnected elements with diverse, multidisciplinary objectives and constraints. The challenge is to develop a mathematical model that will satisfy the special demands of a conceptual/preliminary design group where understanding and innovation are of prime importance. Our model is simple enough to provide quick solutions for understanding, yet complex enough to display features such as spanwise lift distribution and the essential effects of laminated wing design. The study model, shown in Fig. 2, is a cantilevered, elastically coupled beam structure that has three structural stiffness parameters and two characteristic wing deflections, bending and torsion, to describe the static response of a wing to aerodynamic loads.[29,30]

The wing planform geometry shown in Fig. 2 is typical of a low-speed aeroelastic wind-tunnel model. The wing is divided into discrete streamwise panels, as shown in Fig. 3; each panel is defined by its panel width and the streamwise $x$ and cross-streamwise/

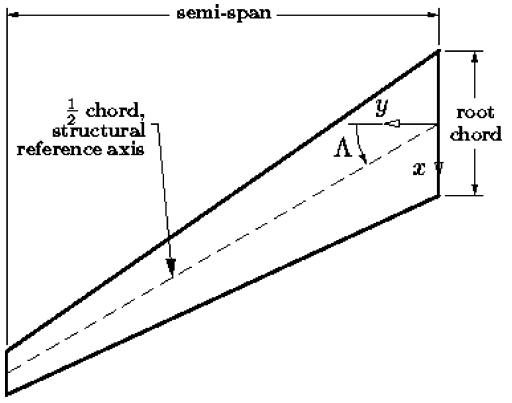


**Fig. 2 Wing planform used for study; root chord 17.74 in. (450.6 mm); aerodynamic aspect ratio 6.53 for the untapered wing (based on the span).**

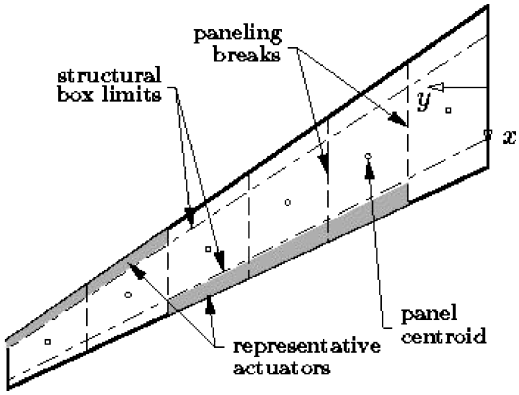


**Fig. 3 Discretized analytical model showing control surface discretization and structure location within the wing.**

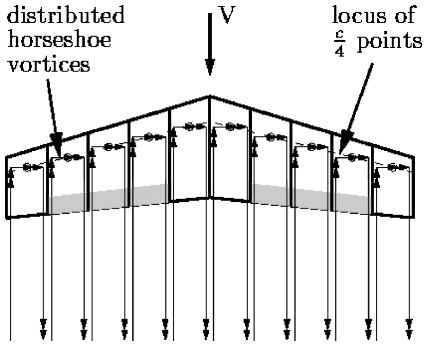


**Fig. 4 Aeroelastic wing aerodynamic model.**

spanwise $y$ location from the wing-root midchord to the panel centroid. The structural stiffness derives from a laminated box-beam whose upper and lower elements carry the aerodynamic load. Continuous, compliant actuators with a flap-to-chord ratio of 0.15 (both leading- and trailing-edge actuators) are represented by discrete elements that surround the structural surface. The aerodynamic portion of the analysis uses a simple, but accurate, aerodynamic model for spanwise lift calculation, as indicated in Fig. 4. The deviation in induced drag from the minimum (elliptical lift distribution) is computed using Fourier-series coefficients to describe the actual lift distribution.

The wing box derives all of its stiffness from advanced composite, laminated wing skin material. This wing-box skin uses an $x' - y'$ coordinate system with the positive $x'$ axis directed aft on the wing; the positive $y'$ axis lies along the swept wing span at the chordwise centerline of the wing as indicated in Fig. 5. The laminate ply angle

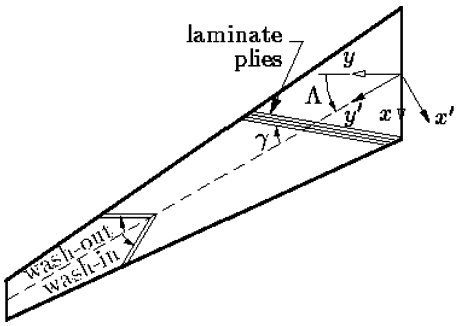


**Fig. 5 Laminate stiffness tailoring parameter definition.**

zero (reference) corresponds to the principal and secondary stiffnesses aligned with the $y'$ and $x'$ axes, respectively, or the primary stiffness along the swept-wing span. The ply angle rotation from this position is $\gamma$, measured positive clockwise as shown.

The relationship between the internal wing-box moment resultants and derivatives of wing deformation is written as follows:

$$\begin{Bmatrix} M \\ T \end{Bmatrix} = \begin{bmatrix} EI & -K \\ -K & GJ \end{bmatrix} \begin{Bmatrix} \partial^2 w/\partial y^2 \\ \partial\theta/\partial y \end{Bmatrix} \tag{1}$$

The flexibility relationship is written as

$$\begin{Bmatrix} \partial^2 w/\partial y^2 \\ \partial\theta/\partial y \end{Bmatrix} = \frac{1}{1-kg} \begin{bmatrix} 1/EI & g/EI \\ g/EI & 1/GJ \end{bmatrix} \begin{Bmatrix} M \\ T \end{Bmatrix} \tag{2}$$

The flexibility matrix must be positive definite, so that $(1 - kg) > 0$. This leads to the definition of the parameter $\Psi^2 = K^2/(EI \cdot GJ) < 1$, which is bounded:

$$-1 < \Psi < 1 \tag{3}$$

This parameter defines the type and extent of the bend-twist deformation coupling. Wash-out laminates (bend-up/twist-down) have negative $K$ (or $\Psi$) values, whereas wash-in laminates (bend-up/twist-up) have positive $K$ values. Negative $K$ parameters are associated with laminated construction with large numbers of plies swept forward of the structural reference axis, as shown in Fig. 5.

## Passive Aeroelastic Induced Drag Reduction

To show how airspeed, sweep angle, and taper ratio affect induced drag, we used our method to calculate the spanwise lift distribution and the resulting induced drag for a wing planform with different laminate ply angles. In each of Figs. 6–8, the fractional drag increase parameter $\delta$ is plotted on the vertical axis, whereas laminate ply angle $\gamma$ is plotted on the horizontal axis. The parameter $\delta$ is the fractional change in induced drag above that for minimum drag (induced drag will not be zero, only a minimum). For instance, $\delta$ equal to 0.10 means that there is a 10% increase in induced drag above the minimum found when the spanwise lift distribution is elliptical. The other independent parameter is airspeed $U_\infty$. Laminate induced washout (negative $K$) is associated with laminate ply angles between 0 and 90 deg, whereas wash-in (positive $K$) corresponds to ply angles between 0 and $-90$ deg. Also note that the starred line in Figs. 6–8 marks ply angle and airspeed combinations for which the wing diverges.

Figure 6 shows that induced drag on the unswept, untapered wing changes with airspeed and might depend strongly on the laminate ply angle and the stiffness coupling created by the laminate design. Aeroelastic distortion on isotropic and orthotropic laminated wings produces twist that tends to load up outboard wing sections and distort any elliptical or near elliptical lift distribution that might have been present at lower airspeeds. Laminate induced washout tends to restore the "good" lift distribution. For some ply angles, the drag change remains small even if the airspeed changes

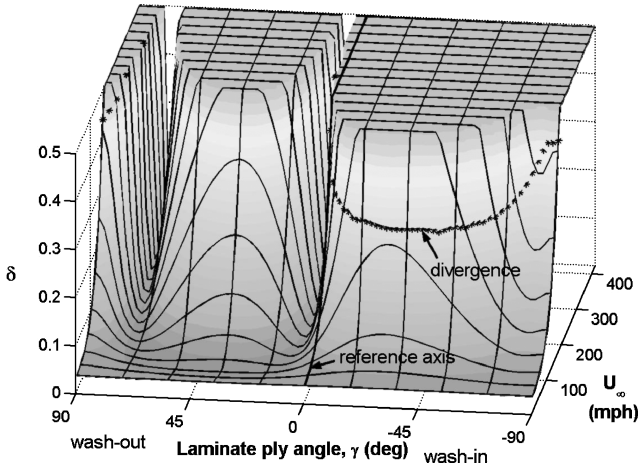


**Fig. 6 Effect of laminate tailoring upon induced drag; untapered, unswept wing with structural aspect ratio 4.7.**

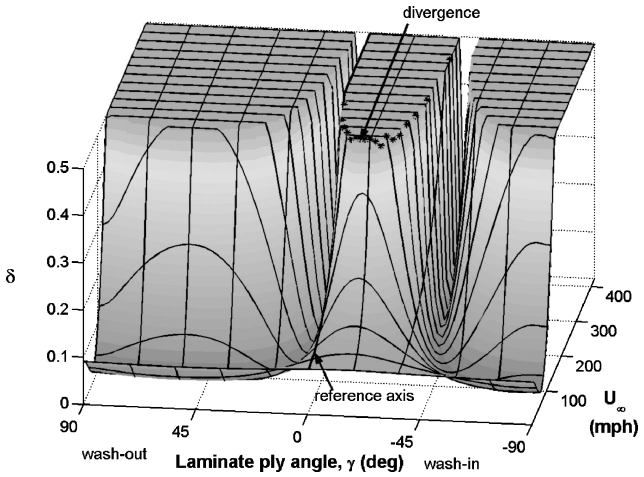


**Fig. 7 Effect of laminate tailoring on induced drag; untapered wing swept aft 30 deg.**

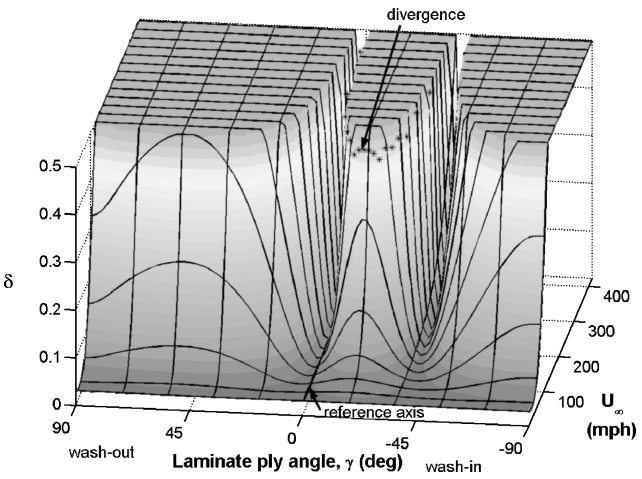


**Fig. 8 Effect of laminate tailoring on induced drag; 30-deg aft swept wing; taper ratio = 0.3.**

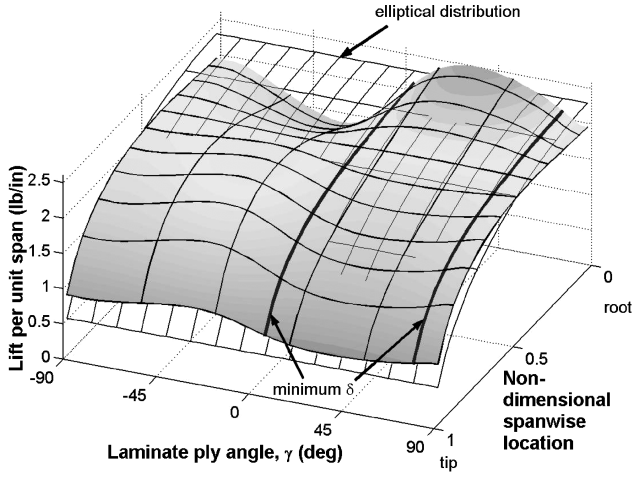


**Fig. 9 Elliptic lift distribution compared to the aeroelastic lift distributions for different laminate ply angles.**

a great deal; these correspond to bottoms of the narrow valleys in Fig. 6.

Laminate aeroelastic tailoring reduces induced drag, but it cannot make $\delta$ equal to zero. When aeroelastic effects are pronounced (at higher airspeeds), the effect of laminate coupling is particularly important because coupling of bend/twist aeroelastic distortion produces large changes in the spanwise lift distribution and, as a result, a large change in induced drag. The valleys in Fig. 6 also become narrower as airspeed increases, indicating that drag sensitivity to laminate orientation increases at higher airspeeds.

The effect of laminate design and orientation on untapered wing-induced drag when the wing is swept aft 30 deg is shown in Fig. 7. The laminate coupling feature that produces the drag reduction for the sweptback wing is wash-in. This is opposite to that observed for the unswept wing.

Finally, Fig. 8 shows the effect of laminate rotation for a 30-deg aft swept wing with taper (similar to the wing planform of Fig. 5). Both taper and positive sweep shift the location of the narrow valleys in the plots toward more pronounced wash-in laminates.

Figure 9 plots both the elliptical and aeroelastic spanwise lift distributions against laminate ply angle for the unswept, untapered wing at a freestream airspeed below the divergence airspeed. The area under each lift distribution curve is constant so that that we have constant wing lift at any laminate design. Note that there is a "hump" in the spanwise lift distribution in the wing outboard region associated with wash-in laminates near $\gamma = 60$ deg; here the wing is close to static divergence.

Figure 9 shows that the lift distribution has two ply angles that create spanwise lift distributions that are nearly elliptical. These two distributions, marked by heavy lines in Fig. 9, correspond to laminates located in the two valleys in Fig. 6. Although these lift distributions are nearly elliptical, Figs. 6–8 show that absolute minimum induced drag ($\delta = 0$) cannot be attained using only aeroelastic stiffness tailoring.

## Active Static Aeroelastic Control

Controller arrays can be used to reshape the wing spanwise lift distribution at all flight speeds to drive the drag parameter $\delta$ to zero and minimize induced drag. However, the distribution of the actuator input and the power required depend on laminate ply angle because laminate angle controls the baseline drag and controls bend/twist coupling that helps or hinders the control surface in its lift distribution shaping mission.

Power required for lift distribution reshaping and drag reduction depends on the aileron (controller) spanwise (or chordwise) location and geometric size. Conventional airplane configurations have only one or two discrete ailerons. However, new adaptive wings have been proposed with smart actuators that extend along the entire leading and trailing edges; their spanwise deflection pattern along the span is continuous and precisely controlled. These actuator arrays include ailerons, leading-edge surfaces, active chordwise cambering, a combination of these three controllers, or other advanced control actuator devices.

Let us examine the wing static aeroelastic equilibrium equations for our wing idealization when it is operating in subsonic flow. These equations provide a matrix expression for spanwise lift as a function of wing spanwise angle-of-attack distribution (including aeroelastic effects) and control surface deflections. The static equilibrium of forces and moments along the wing reference axis is written in matrix form as[30,31]

$$[(1/q)[A_{ij}] - [C_{ij}]]\{l_j\} = \{\alpha_r\} + [[Z_{ij}] + q[E_{ij}]]\{\beta_j\} \quad (4)$$

The matrix $[B_{ij}] = [(1/q)[A_{ij}] - [C_{ij}]]$ is the aeroelastic flexibility matrix for the symmetrical, cantilevered wing. This matrix is a function of the distribution of aerodynamic derivatives along the wing, either estimated or measured, as well as planform geometry and structural stiffness. The distribution of known initial angles of attack along the wing is given by $\{\alpha_r\}$ (a rigid-body angle distribution), whereas the distribution of control surface deflections is given by $\{\beta_i\}$. In our studies we used a constant angle for the distribution of $\{\alpha_r\}$ so that all wing sections had the same initial angle before they were loaded. The matrices $[Z_{ij}]$ and $[E_{ij}]$ are functions of controller aerodynamic derivatives, location, and wing stiffness. We rewrite Eq. (4) as

$$[B_{ij}]\{l_j\} = \{\alpha_r\} + [[Z_{ij}] + q[E_{ij}]]\{\beta_j\} \quad (5)$$

so that the lift distribution is

$$\{l_i\} = [B_{ij}]^{-1}\{\alpha_r\} + [B_{ij}]^{-1}[[Z_{ij}] + q[E_{ij}]]\{\beta_j\} \quad (6)$$

This lift distribution is used to estimate the induced drag at this flight condition. Equations (5) and (6) are key relationships; we can treat one of the three sets of variables ($\{\alpha_r\}$, $\{\beta_i\}$, or $\{l_i\}$) as an unknown, whereas the other two are known inputs. In Eq. (6) the lift distribution is the unknown; for drag reduction $\{\beta_i\}$ is the unknown.

Our design objective is to combine aeroelastic tailoring and active control surfaces to change the uncontrolled lift distribution to an elliptical spanwise lift distribution (or any other distribution favored by the designer). With full-span ailerons, full-span leading-edge devices, or full-span camber bending, a closed-form solution for the control deflections necessary to produce an elliptical lift distribution for minimum drag results from Eq. (5)

$$\{\beta_i\} = [[Z_{ij}] + q[E_{ij}]]^{-1}[[B_{ij}]\{l_j\}_{\text{elliptical}} - \{\alpha_r\}] \quad (7)$$

With wing camber bending control, or other advanced control scheme, the spanwise distribution of active camber $\{\varepsilon/c\}$ or other controller input replaces $\{\beta_i\}$ in Eq. (7), whereas the aerodynamic derivatives with respect to camber or controller input replace those used in the matrices $[Z_{ij}]$ and $[E_{ij}]$ for the continuous compliant aileron.[31]

To illustrate how laminate tailoring can reduce control surface deflections necessary to create an elliptic lift distribution, we chose a laminated wing with 30-deg sweep, aileron flap-to-chord ratio 0.15 and a taper ratio of 0.30. Figure 10 is typical of the amount of trailing-edge deflection required when full-span continuous ailerons are used to create an elliptical spanwise lift distribution. Results were calculated at two different subsonic Mach numbers, $M = 0.2$ and $M = 0.4$, at sea level. The wing laminated structural box has 60% of its outer plies rotated an amount $\gamma$.

Note that the orthotropic laminate design ($\gamma = 0$) requires large aileron deflections at low and high speeds; the aileron deflection distribution changes with airspeed because of aeroelastic effects. Figure 10 shows that a laminate design with $-21.6$ deg (wash-in) can control induced drag with small surface deflections. These results are consistent with previous results that indicate that wash-in ($+K$) is desirable for drag reduction for aft swept wings.

Although the results shown in Fig. 10 can be used to identify the best laminate design, it is better to use a formal metric to evaluate the controller effectiveness. Energy or power required to operate,

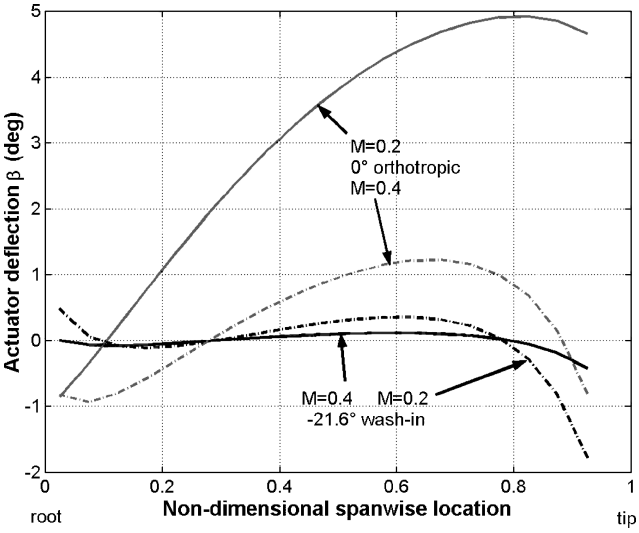


**Fig. 10 Aileron deflection angles needed to minimize induced drag; 30-deg swept wing, flap-to-chord ratio of 0.15; taper ratio 0.30.**

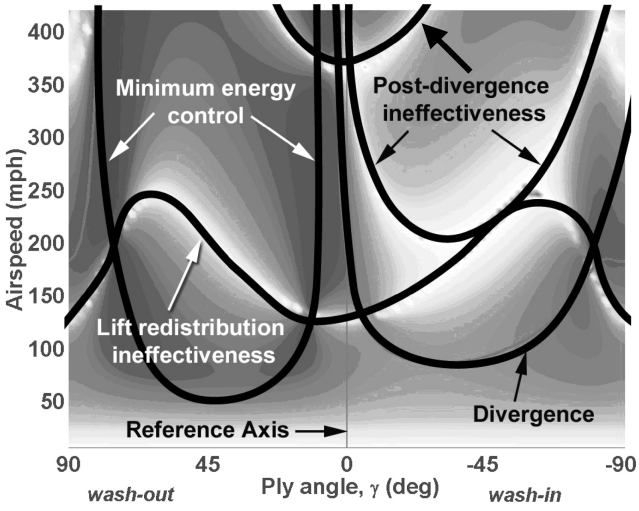


**Fig. 11 Influence of laminate tailoring and airspeed on actuator deflections for induced drag minimization, showing small and large deflection designs. Uniform planform wing design.**

deflect, or deform the control surfaces is a good choice. However, the information necessary to compute power and energy is not available at this stage of design. However, energy input to the actuators is related to their rotational deformation. As a result, we chose a weighted actuator effort parameter that is sum of the squares of controller deflection. For our present model this metric is defined as an effort metric,

$$\upsilon = \sqrt{\sum_i W_i \beta_i^2}$$

Figure 11 is a top view of a three-dimensional plot with three parameters: the effort metric $\upsilon$ (plotted out of the page), laminate ply angle $\gamma$, and airspeed $U_\infty$. The curves labeled "minimum energy control" in Fig. 11 are associated with valleys in which relatively small values of control effort $\upsilon$ required to create an elliptical lift distribution. The laminate designs that correspond to these minimum effort valleys are the same laminate designs that produce the minimum $\delta$ valleys in Figs. 6–8, without active control. Also identified is divergence static instability combinations.

The two curves in Figure 11 marked "lift redistribution ineffectiveness" and "postdivergence ineffectiveness" trace out ridges with large values of $\upsilon$. A third curve at the top of Fig. 11 also identifies the same effect. These three curves locate combinations of airspeed and laminate angles where the actuator energy to create an elliptic lift distribution is extremely large (or even infinite, implying that the control cannot create changes in lift with these combinations). These regions are much like classical aileron reversal regions. If the second term on the right-hand side of Eq. (4) is set equal to zero, the control ineffectiveness condition labeled "lift redistribution ineffectiveness" in Fig. 11 is reproduced. Note that this locus is predicted by an eigenvalue problem, written as

$$[E_{ij}]^{-1}[Z_{ij}]\{\beta_j\} = -q_0\{\beta_j\} \tag{8}$$

At this dynamic pressure $q_0$, there is a self-equilibrating deflection shape $\{\beta_i\}$ that places the wing in static equilibrium without changing the wing lift distribution, no matter what the magnitude of the control deflection.

At a flight dynamic pressure corresponding to the lowest value eigenvalues in Eq. (8), the control surface deflection pattern to create an elliptical lift distribution has a large component of the first eigenvector of the problem defined in Eq. (8). As a result, very large control deflections are necessary to create the elliptical distribution. When the dynamic pressure is increased, the aileron deflections for minimum drag reverse and are opposite to those found at slightly lower airspeeds.

This behavior is a reversal-like phenomenon peculiar to this drag-reduction objective. The combination of control surfaces to create a drag-reduction control law can create a deformation shape along the wing that is statically stable, but whose aeroelastic forces and moments create no net lift. There are as many deformation forms as there are degrees of freedom, but each deformation form has a special dynamic pressure associated with it because the effect is aeroelastic.

## Optimization Problem

To identify and refine wing structural designs, we need high-fidelity models and a more sophisticated approach than that discussed earlier. The well-defined minimum induced drag "valleys" in Figs. 6–8 suggest the definition of a formal optimization problem to find the best laminate ply orientation to reduce drag. The minimum induced drag valleys of Fig. 6 and the minimum control effort valleys of Fig. 11 occur at nearly the same laminate angles. Finding the minimum induced drag laminate design and then adding the active controls gives a good controller design very near the minimum energy and power requirements for the cases we examined. On the other hand, there is no assurance that this will be the case for other classes of wings.

It appears that an effective approach is a sequential approach in which we first find the optimum laminate design and then solve a second optimization problem to find control surface deflections. The formal optimization problem for laminate angles is stated as follows:

Minimize:

$$\delta(\gamma)$$

Subject to:

$$\gamma_{\min} < \gamma < \gamma_{\max}$$

$$U_\infty = x \text{ miles/hour (the design flight speed)}$$

A one-dimensional search algorithm, such as the Golden Section method, can solve this optimization problem. As indicated in Figs. 6–8, the design space is nonconvex; as a result, optimization can favor a local minimum over the global minimum. Starting the optimization from several initial guesses allows us to find and compare both minima.

The induced drag minimizing laminate design was found using a modified Golden Section method[32] at several airspeeds for the unswept, untapered wing model. The results are summarized in Table 1.

**Table 1 Optimum laminate designs with corresponding induced drag parameter $\delta$ at several airspeeds; unswept, untapered wing**

| Airspeed, mph | $\gamma_{\text{opt}}$ (global), deg | $\delta_{\min}$ (global) | $\gamma_{\text{opt}}$ (local), deg | $\delta_{\min}$ (local) |
|---|---|---|---|---|
| 60 | 39.7 | 0.017 | 39.7 | 0.017 |
| 180 | 75.3 | 0.021 | 7.9 | 0.029 |
| 300 | 77.3 | 0.036 | 6.6 | 0.071 |
| 420 | 77.8 | 0.077 | 6.2 | 0.203 |

**Table 2 Comparison of induced drag with optimum and fixed laminate designs at several airspeeds; unswept, untapered wing**

| Airspeed, mph | $\gamma_{\text{opt}}$ (420 mph), deg | $\gamma_{\text{opt}}$, deg | $\delta_{\min}$ ($\gamma_{\text{opt@420mph}}$) | $\delta_{\min}$ | % increase compared to absolute minimum |
|---|---|---|---|---|---|
| 60 | 77.8 | 39.7 | 0.031 | 0.017 | 82.4 |
| 180 | 77.8 | 75.3 | 0.032 | 0.021 | 52.4 |
| 300 | 77.8 | 77.3 | 0.040 | 0.036 | 11.1 |
| 420 | 77.8 | 77.8 | 0.077 | 0.077 | 0.0 |

Note that at the higher airspeeds the optimum laminate design is nearly constant over a range of airspeeds. Table 2 compares the global minimum induced drag parameter at different design airspeeds to the induced drag parameter found if the highest airspeed is chosen as the design speed for the laminate tailoring. Choosing a laminate design using the highest flight speed causes an increase in $\delta$ compared to the best laminate designs at lower flight speeds. The greatest difference is at the lower airspeeds. However, choosing a design airspeed in the midrange of airspeeds results in large increases in $\delta$ at higher speeds.

## Induced Drag Minimizing Actuator Deflections

We have demonstrated the ability of a formal optimization method to locate laminate orientations to minimize drag. The second part of the problem is to find the controller deformations to further reduce drag. We have previously done this by developing a closed-form solution to this problem. However, it is necessary to use formal optimization to find induced drag minimizing control surface rotations instead of relying on the closed-form solution presented in Eq. (7) in cases that include 1) actuator deflection limits; 2) cases in which the number of controllers exceeds the number of equations, for example, both leading-edge and trailing-edge devices used simultaneously; and 3) use of partial span control surfaces where there are fewer controllers than equations.

For full-span compliant or segmented actuators, the actuator deflection distribution must be changed with design flight speed. For a given structural design, the control deflection optimization problem can be formally stated as follows:

Minimize:

$$\delta(\beta_j)$$

Subject to inequality constraints:

1)

$$\left|\{1\}^T[B_{ij}]^{-1}[[Z_{ij}] + q[E_{ij}]]\{\beta_j\}\right| - \varepsilon \le 0$$

with

2)

$$-5\,\text{deg} < \beta_j < 5\,\text{deg}$$

and

3)

$$U_\infty = x \text{ miles/hour (design flight speed of interest)}$$

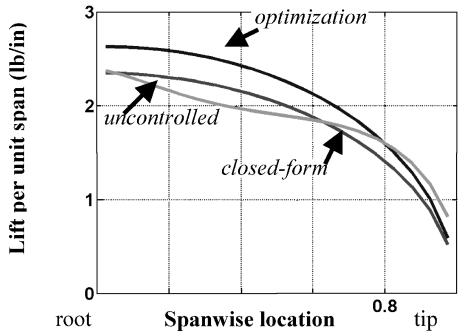


**Fig. 12 Comparison of closed-form and underconstrained optimization lift distributions.**

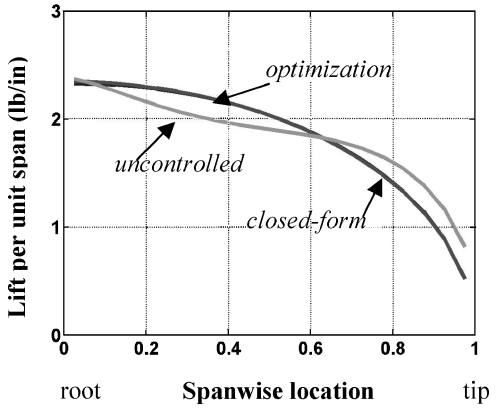


**Fig. 13 Comparison between closed-form and fully constrained optimization lift distributions.**

The inequality constraint 1) is necessary to ensure that the total lift on the wing is constant during optimization. This constraint sums the additional lift produced by the actuator deflections and restricts it to be nearly zero, to within a small number $\varepsilon$. Although setting $\varepsilon$ to zero would constrain the total additional lift to be exactly zero, the sequential-quadratic-programming optimization algorithm used in this study[32] behaves better and finds the solution faster if $\varepsilon$ is set to a small number (e.g., $10^{-4}$).

Figure 12 shows optimization results obtained without the first constraint, using only maximum surface deflection as a constraint. The total lift after optimization is elliptical, but it is greater than the uncontrolled lift. When the first constraint is added, the results are identical to the closed-form solution, as shown in Fig. 13.

## Conclusions

Designing a stiffness tailored structure that deforms to produce a nearly elliptical lift distribution can reduce induced drag. This appears to be particularly effective at high subsonic airspeeds where aeroelastic effects are more pronounced. Active control, coupled with laminate stiffness tailoring of the wing structure, can further reduce induced drag with small actuator deformations. A closed-form solution exists for the actuator input to minimize induced drag at subsonic airspeeds.

At some airspeeds, controllers become ineffective when required to redistribute the spanwise lift distribution to create an elliptical lift distribution. These airspeeds can be determined by solution of an eigenvalue problem. Formal optimization techniques can help the designer to identify laminate stiffness combinations and full-span compliant actuator deformations when the closed-form solution does not produce a satisfactory answer.

## Acknowledgments

Trent Logan of Boeing/Long Beach provided essential information and ideas during the early phases of this research. The authors appreciate the advice and active support provided by Vipperla Venkayya of Air Force Research Laboratory/VA.

## References

[1]Weisshaar, T. A., Nam, C. H., and Batista-Rodriguez, A., "Aeroelastic Tailoring for Improved UAV Performance," AIAA Paper 98-1757, April 1998.

[2]Duke, D. K., "Induced Drag Reduction Using Aeroelastic Tailoring and Adaptive Control Surfaces," M.S. Thesis, School of Aeronautics and Astronautics, Purdue Univ., West Lafayette, IN, May 2000.

[3]Shirk, M. H., Hertz, T. J., and Weisshaar, T. A., "Aeroelastic Tailoring-Theory, Practice, Promise," *Journal of Aircraft*, Vol. 23, No. 1, 1986, pp. 6–18.

[4]Braymen, W. W., Rogers, W. A., and Shirk, M. H., "Wind Tunnel Test and Aerodynamic Analysis of Three Aeroelastically Tailored Wings," *Proceedings of the 13th Congress of the Aeronautical Sciences*, 1982.

[5]Rodden, W. P., Surber, T. E., and Vetter, H. C., "The Effect of Flexibility on the Drag Polar of an Aircraft," *Journal of the Aeronautical Sciences*, June 1957, pp. 456, 457.

[6]Rodden, W. P., "Static Aeroelasticity in Combat Aircraft—Secondary Considerations of Static Aeroelastic Effects on High Performance Aircraft," *Proceedings of the Static Aeroelasticity in Combat Aircraft*, 1985, p. 42.

[7]Munk, M. M., "The Minimum Induced Drag of Airfoils," NACA TR 121, 1921.

[8]Jones, R. T., *Wing Theory*, Princeton Univ. Press, NJ, 1990, pp. 105–114.

[9]Elber, W., "Means for Controlling Aerodynamically Induced Twist," U.S. Patent 4,330,100, 18 May 1982.

[10]Ferris, J. C., "Wind-Tunnel Investigation of a Variable Camber and Twist Wing," NASA TND-8475, Aug. 1977.

[11]Gilbert, W. W., "Mission Adaptive Wing System for Tactical Aircraft," *Journal of Aircraft*, Vol. 18, No. 7, 1981, pp. 597–602.

[12]Waddoups, M. E., Smith, C. B., and McMickle, R. W., "Composite Wing for Transonic Improvement; Vol. I—Composite Wing Aeroelastic Response Study," Air Force Flight Dynamics Laboratory, AFFDL-TR-71-24, Wright–Patterson AFB, OH, 1972.

[13]Levinsky, E. S., Schappelle, R. H., and Pountney, S., "Airfoil Optimization Through the Adaptive Control of Camber and Thickness," Convair, CASD-NSC-75-004, Sept. 1975.

[14]Levinsky, E. S., et al., "Wind Tunnel Test of an Improved Computer-Controlled Variable-Geometry Wing (Self-Optimizing Flexible Technology Wing Program)," Arnold Engineering Development Center, AEDC-TR-80-42, 1981.

[15]Renken, J. H., "Mission Adaptive Wing Camber Control Systems for Transport Aircraft," AIAA Paper 85-5006, Oct. 1985.

[16]Hall, J. M., "Executive Summary AFTI/F-111 Mission Adaptive Wing," Flight Dynamics Lab., WRDC-TR-89-3083, Wright–Patterson AFB, OH, Sept. 1989.

[17]Gilyard, G., "Development of a Real-Time Transport Performance Optimization Methodology," AIAA Paper 96-0093, Jan. 1996.

[18]Weisshaar, T. A., and Ehlers, S. M., "Adaptive Aeroelastic Composite Wings—Control and Optimization Issues," *Composites Engineering*, Vol. 2, No. 5–7, 1992, pp. 457–476.

[19]Muller, M. B., and Weisshaar, T. A., "Maximizing Deflections Produced by Induced Strain Beam-Like Actuators for Transonic Drag Reduction," *Proceedings of the AIAA/ASME Adaptive Structures Forum*, AIAA, Washington, DC, 1994, pp. 388–401.

[20]Miller, G., "Active Flexible Wing (AFW) Technology," Wright Aeronautical Lab., AFWAL-TR-87-3096, Wright–Patterson AFB, OH, 1988.

[21]Pendleton, E. E., Lee, M., and Wasserman, L., "Application of AFW Technology to the Agile Falcon," *Journal of Aircraft*, Vol. 29, No. 3, 1992, pp. 444–451.

[22]Miller, G., "An Active Flexible Wing Multidisciplinary Design Optimization Method," *Proceedings of the 5th AIAA Symposium on Multidisciplinary Analysis and Optimization*, AIAA, Washington, DC, 1994.

[23]Perry, B., Cole, S., and Miller, G., "A Summary of the AFW Program," *Journal of Aircraft*, Vol. 32, No. 1, 1995, pp. 10–15.

[24]Khot, N., Eastep, F., and Kolonay, R., "Optimization of a Composite Wing Structure for Enhancement of the Rolling Maneuver," *Proceedings of the 6th AIAA/NASA/ISSMO Symposium on Multidisciplinary Analysis and Optimization*, AIAA, Reston, VA, 1996, pp. 152–161.

[25]Yurkovich, R., "Optimum Wing Shape for an Active Flexible Wing," *Proceedings of the AIAA/ASME/ASCE/AHS 36th Structures, Structural Dynamics and Materials Conference*, AIAA, Washington, DC, 1995.

[26]Eastep, F. E., "Development of Preliminary Design Models for Active Aeroelastic Wing Application," Air Force Wright Laboratory, AFWL-TR-97-3019, 1997.

[27]Monner, H. P., Sachau, D., and Breitbach, E., "Design Aspects of the Elastic Trailing Edge for an Adaptive Wing," North Atlantic Treaty Organization (NATO) Specialists Meeting: Structural Aspects of Flexible Aircraft Control, Oct. 1999.

[28]Tulinius, J., "Active Flexible Wing Aircraft Control System," U.S. Patent 5,082,207, 21 Jan. 1992.

[29]Weisshaar, T. A., "Forward Swept Wing Static Aeroelasticity," Air Force Flight Dynamics Lab., AFFDL-TR-79-3087, Wright–Patterson AFB, OH, June 1979.

[30]Gray, W., and Schenk, K., "A Method for Calculating the Subsonic Steady-State Loading on an Airplane with a Wing of Arbitrary Plan Form and Stiffness," NACA-TN-3030, July 1953.

[31]Katz, J., and Plotkin, A., *Low-Speed Aerodynamics: From Wing Theory to Panel Methods*, McGraw–Hill, New York, 1991. pp. 122–139.

[32]Vanderplaats, G. N., *Numerical Optimization Techniques for Engineering Design*, 3rd ed., Vanderplaats Research and Development, Inc., Colorado Springs, CO, 1999, pp. 241–247.